Femtosecond Self-Reconfiguration of Laser-Induced Plasma Patterns in Dielectrics

Jean-Luc Déziel,[1] Louis J. Dubé,[1,*] Sandra H. Messaddeq,[2] Younès Messaddeq,[2] and Charles Varin[3]

[1] *Département de physique, de génie physique et d'optique, Université Laval, Québec G1V 0A6, Canada*
[2] *Centre d'Optique, Photonique et Laser, Université Laval, Québec, Québec G1V 0A6, Canada*
[3] *Département de physique, Université d'Ottawa, Ontario K1N 6N5, Canada*

Laser-induced modification of transparent solids by intense femtosecond laser pulses allows fast integration of nanophotonic and nanofluidic devices with controlled optical properties. So far, the local and dynamic nature of the interactions between plasma and light needed to correctly explain nanograting fabrication on dielectric surfaces has been missing in the theoretical models. With our numerical approach, we show that a self-consistent dynamic treatment of the plasma formation and its interaction with light triggers an ultrafast reconfiguration of the periodic plasma patterns on a field-cycle time scale. Within this framework, a simple stability analysis of the local interactions explains how the laser-induced plasma patterns change their orientation with respect to the incident light polarization, when a certain energy density threshold is reached. Moreover, the reconfigured sub-wavelength plasma structures grow into the bulk of the sample and agree with the experimental findings of self-organized volume nanogratings. Mode coupling of the incident and transversally scattered light with the periodic plasma structures is sufficient to initiate the growth and the self-organization of the characteristic pattern with a periodicity of a half-wavelength in the medium.

PACS numbers: 52.35.Qz, 52.65.-y, 79.20.Eb, 81.16.Rf

arXiv:1702.02480v2 [physics.optics] 9 Feb 2017

Laser micro-machining of transparent material by femtosecond pulses promises fast integration of 2D and 3D nanophotonic and nanofluidic devices with tailored properties [1–4]. Exposition of solid materials to intense laser radiation typically gives rise to complex light-matter interaction processes like high harmonic generation [5], ionization avalanche breakdown [6], and ultrafast plasma dynamics [7]. Such nonlinear light-matter interaction processes are often associated with instabilities that lead to the formation of periodic surface and bulk patterns [8, 9]. Thus far, static surface mode analysis has successfully explained the origin and characteristics of periodic patterns formed on laser-processed metals and semi-conductors [9, 10]. However, better understanding of femtosecond laser-plasma interaction dynamics is necessary to explain nanograting formation in dielectrics, where predictions from current theoretical models are inconsistent with respect to experimental observations on several important aspects.

Extensive experimental and theoretical studies have examined a number of laser-induced nanostructures that arise from the interaction between intense femtosecond laser pulses and materials. In particular, laser-induced periodic surface structures (LIPSS) have been studied with the Sipe theory [11] and explained as the result of interference patterns between the incident light and static surface modes triggered by surface inhomogeneities. A large number of experimentally observed LIPSS on lossy materials are correctly described within this framework [10]. For transparent dielectrics, Sipe theory is only valid in the early ionization stage, where the plasma density is fairly low. During the ionization avalanche, transient optical properties, referred to *intrapulse feedback*, have to be taken into account to allow for self-interaction and therefore, self-organization of the plasma patterns while the plasma is being formed. An extended Sipe theory with a plasma density that is homogeneous in both space and time has been explored [12, 13], but this approach does not account for the self-interaction of plasma structures.

Studies that accounted for the time and space dependence of the plasma density have focused on volume interactions, and they indeed permit the self-organization of plasma patterns in the bulk of dielectric materials [8, 14, 15]. However, the simulations that tested the proposed theoretical *nanoplasmonic* model predicted plasma growth in the direction opposite to the laser propagation, with periodic width oscillations along the same axis. In contrast, experiments show that structures grow towards the laser propagation direction with a constant width [3].

Light-matter interaction feedback can also occur between subsequent laser pulses, referred to as *interpulse feedback* [16, 17]. The target can be structurally modified by each laser pulse by mechanisms like ion removal, chemical bonding reconfiguration, melting, hydrodynamic flow, crystallization, amorphization, and so on [18, 19]. The next laser pulses then interact with these permanent modifications and interfere constructively or destructively with them. Interpulse mechanisms result from the energy distribution after irradiation, itself determined by intrapulse dynamics. Therefore, laser-plasma interplay on the single-pulse scale has to be fully understood first, before attempting a complete description of nanostructures fabricated with multiple laser pulses.

In this Letter, we numerically study the spatio-temporal dependence of the near-surface plasma density within a single femtosecond laser pulse interaction in a dielectric medium. We observe an ultrafast reconfiguration of the plasma distribution when the conditions for self-organization are met. This confirms that a dy-

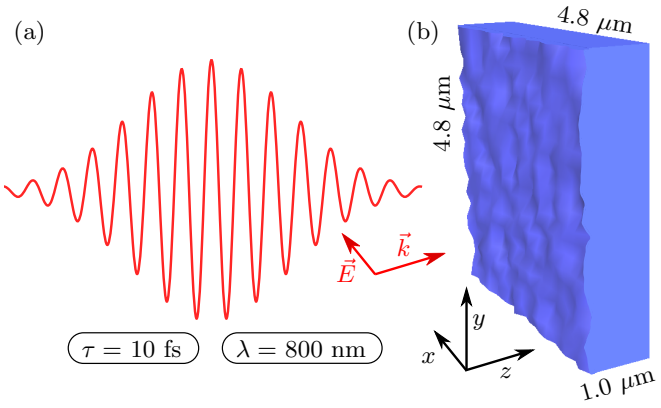

Figure 1. Schematic illustration of the simulations. In (a), the laser pulse is linearly polarized along the x-axis and propagates towards the $+z$-axis. It hits, with normal incidence, a fused silica sample with a rough surface, shown in (b).

namical three-dimensional treatment of the plasma density is crucial to extend the LIPSS theory to transparent medium. Moreover, we obtain plasma growth in the same direction as the laser propagation with constant width, in agreement with experimental observations of volume nanogratings [3]. We find that plasma growth along the propagation axis is correctly described when intrapulse self-organization is dominated by transverse reflections with previously formed plasma structures, instead of longitudinal reflections, as in the current nanoplasmonic model.

Simulations. We solve Maxwell equations with the finite-difference time-domain (FDTD) method [20]. The material affects the field via three currents. (i) Bounded currents $\vec{J}_b = \epsilon_0 \partial(\chi^{(1)}\vec{E} + \chi^{(3)}\vec{E}^3)/\partial t$ account for first and third order susceptibilities (see [21] for details). (ii) Free carriers currents $\vec{J}_f = \omega_p^2/(-\omega^2 + i\omega\gamma)\vec{E}$ account for plasma absorption with $\omega_p^2 \propto \rho/m_e^*$, where ρ is the time and space dependent plasma density that evolves as

$$\partial\rho/\partial t = \left(\nu^K + \rho\nu^C\right)(\rho_0 - \rho)/\rho_0. \qquad (1)$$

Considering only first ionization, the plasma density saturates at the molecular density ρ_0. The field ionization rate ν^K accounts for multiphoton and tunnel ionization mechanisms and is calculated with the Keldysh model adapted for transparent material with a bandgap Δ_g [22]. The collisional ionization $\nu^C = \alpha I$ is proportional to the field intensity for ultrashort laser pulses [6]. (iii) The third current accounts for field energy losses due to field ionization, calculated with $\vec{J}_K = \Delta_g \nu^K (\rho_0 - \rho)\vec{E}/I$.

In our simulations, material parameters are chosen to reproduce the fused silica optical properties; first and third order susceptibilities $\chi^{(1)} = 1.1025$ (refractive index $n = 1.45$), $\chi^{(3)} = 2 \cdot 10^{-22}$ m^2/V^2, plasma damping $\gamma = 10^{15}$ s^{-1}, reduced mass of the electron $m_e^* = 0.8 m_e$, molecular density $\rho_0 = 2.2 \cdot 10^{22}$ cm^{-3}, band-gap $\Delta_g = 9$ eV and collisional cross-section $\alpha = 10$ cm^2/J [6]. The target is a square of side 4.8 μm with a thickness of 1 μm. Surface roughness is mimicked by randomly adding 0 to 20 nm of material over the surface. The laser source is a $\lambda = 800$ nm plane wave linearly polarized along the x-axis propagating along the $+z$-axis. Laser pulses have a gaussian time envelope of duration $\tau = 10$ fs and laser fluences between 1 and 6 J/cm^2. Spatial discretization parameters are $\delta_{x,y} = 20$ nm and $\delta_z = 2$ nm, with time step $\delta_t = 6.33 \cdot 10^{-3}$ fs. The geometry of the simulations is schematized in Fig. 1.

Our most striking result is an ultrafast reconfiguration of the plasma pattern occurring during the ionization avalanche [see Fig. 2(a)-(d)]. The plasma structures initially oriented parallel ($\parallel$) to the laser polarization and with a periodicity $\Lambda_\parallel \sim \lambda/n$ change to orthogonal ($\perp$) structures with $\Lambda_\perp \sim \lambda/2n$ within a few optical cycles, where n is the refractive index. This transition occurs when the laser fluence is high enough for the plasma to reach critical density $\rho/\rho_0 \sim 8\%$, defining a fluence threshold $F_{\rm th}$. These two patterns are commonly observed in experiments with dielectrics and the theory has never been able to account for both of them in a single framework. Whereas LIPSS theory predicts the former pattern $\Lambda_\parallel \sim \lambda/n$, the nanoplasmonic model predicts the latter $\Lambda_\perp \sim \lambda/2n$.

Before the reconfiguration. In the early stage of the interaction [see Fig. 2(a)], the plasma density is still too low for the transient optical properties to cause noticeable feedback and induce self-reorganisation. In this regime, Sipe's static surface mode analysis [11] describes correctly the early plasma growth and emergence of periodic plasma patterns with $\Lambda_\parallel \sim \lambda/n$. These structures result from the interference between the incident light and the scattered radiation off the surface inhomogeneities. We show below that this characteristic pattern appears when intrapulse feedback is missing, which happens if : i. the ionization avalanche has not kicked in yet, ii. the laser fluence is below threshold, or iii. the feedback has been artificially turned off, as we have done to produce Fig. 2(f).

Reflections off the inhomogeneous plasma density. The electrostatic, nanoplasmonic model currently used to explain the formation of periodic patterns in the bulk relies on an initial distribution of nanovoids to initiate the growth of self-organized plasma patterns with $\Lambda_\perp \sim \lambda/2n$ [8]. Recent simulations [14, 15] have shown that, around these nanovoids, spherical nanoplasmas initially grow, causing strong optical reflections and the formation of standing waves along the longitudinal direction. These standing waves are responsible for further plasma growth in the direction opposite to the laser propagation, in contradiction with experiments [3]. We have therefore abstained from the use of nanovoids, but we have nevertheless investigated the relative importance of the longitudinal and transverse reflections within our approach.

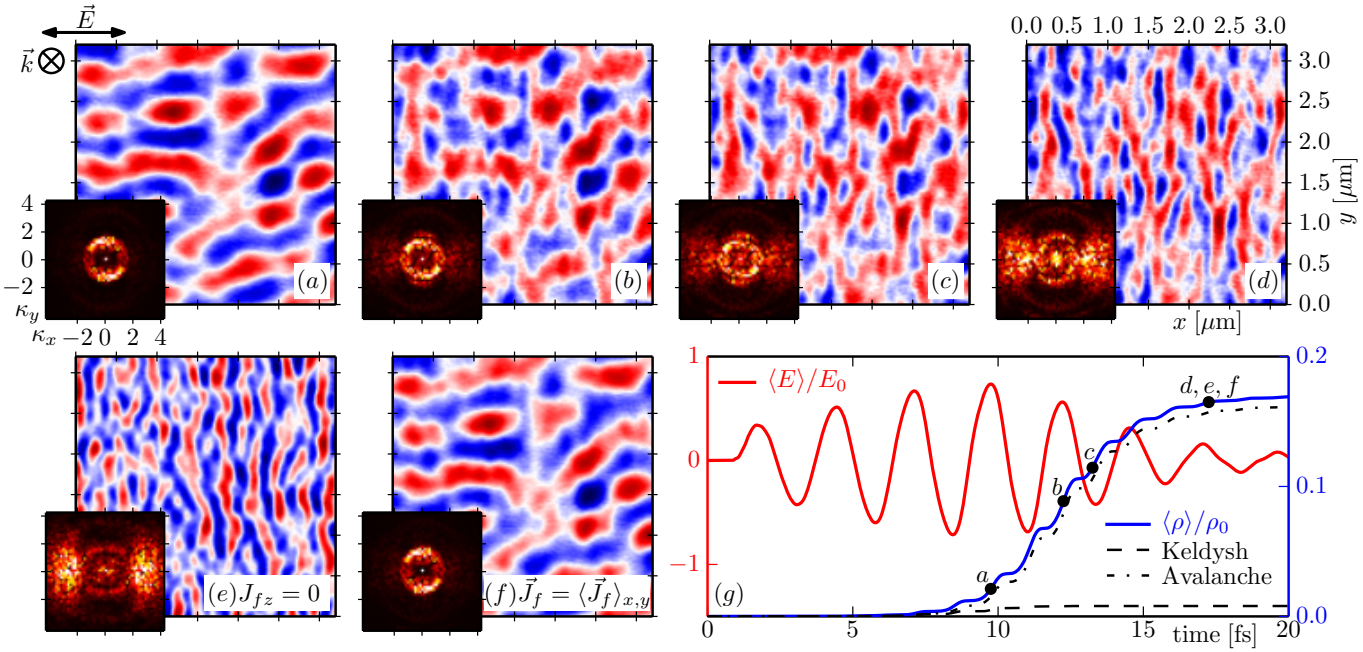

Figure 2. Top row (a) to (d) : Time evolution of the variations in plasma density $\rho(x, y, z)$ (from blue minima to red maxima) at fixed depth $z = 140$ nm with $\tau = 10$ fs and $F = 3$ J/cm^2 $> F_{\text{th}}$ showing the structural transition from $\Lambda_{\parallel} \sim \lambda/n$ to $\Lambda_{\perp} \sim \lambda/2n$. Overlayed subfigures show the 2D Fourier transforms of the corresponding figure. Wavenumbers in the Fourier space $\vec{\kappa}$ are all in units of λ^{-1}. Bottom row : Final plasma structures when reflections are turned off along z (e) or x and y (f). In (g), mean values of normalized E and ρ together with the two contributing ionization mechanisms. The black dots indicate the times of the snapshots (a) to (f).

To test the role of longitudinal reflections in our simulations, we have excluded the z component of $\vec{J}_f$ in the full simulation and obtained Fig. 2(e), where the self-organized and reconfigured plasma structures of Fig. 2(d) are still present. This means that self-organization is here achieved *without* the need of longitudinal reflections, previously thought to be necessary for the formation of bulk patterns [15]. In contrast, transverse reflections along both orthogonal directions x and y can also be turned off by averaging the free currents $\vec{J}_f(x, y, z)$ over the (x, y) plane, at every time step of the simulation. The corresponding final plasma distribution is shown in Fig. 2(f). It is almost identical to Fig. 2(a), which indicates that without transverse reflections, pattern reconfiguration does not occur.

Laser-plasma interplay. Reflections against local maxima in the plasma density scatter light in the transverse plane. This scattered light couples to the natural modes associated with the plasma density patterns. The interplay between this transversely scattered light, the plasma density, and the incident light may be additive (positive feedback) or subtractive (negative feedback), which leads to the growth or inhibition of periodic structures in both x and y directions. Therefore, the ultrafast pattern reorganization shown in Fig. 2 can be explained by a metallic waveguide approach, already believed to be linked to self-organized plasma patterns (see, e.g., [23]).

A consequence of the dynamic laser-plasma interplay just described is the self-inhibition, during ionization avalanche, of the early $\parallel$-structures shown in Figs. 2(a) and 3(a). We recall that this type of structures, whose origin is explained by Sipe [11], appears when the plasma density is low and intrapulse interaction feedback is negligible. However, our simulations show that these structures are dynamically suppressed when the plasma approaches critical density. Our interpretation is the following. (i) The local maxima of the early $\parallel$-structures effectively serve as waveguide boundaries between which the lowest-order transverse electric (TE_1) resonant modes develop. (ii) The field distribution of these TE_1 modes is maximum halfway between the walls, where ionization is locally enhanced. The early plasma density distribution then becomes anti-correlated with ionization, i.e., a negative feedback loop drives the distribution towards a nearly-flat equilibrium [see Figs. 2(b,c) and 3(b) where the $\parallel$-structures have essentially vanished].

In the orthogonal orientation, the plasma distribution is initially flat in the bulk, as shown in Fig. 3(c). However, this equilibrium becomes unstable when feedback starts to manifest itself. As soon as the symmetry of the incident plane wave breaks, some energy will fall into the lowest-order non-uniform transverse magnetic (TM_1) resonant modes. Since the TM_1 mode has antinodes located at the maxima of the local plasma density, a positive feed-

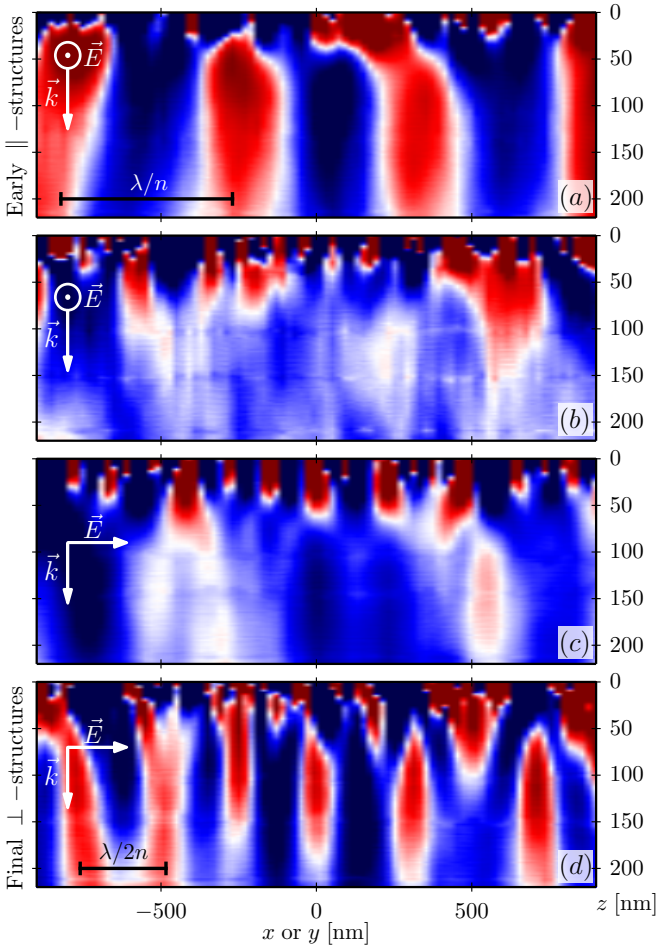

Figure 3. Transverse views of the relative variations in the plasma density (from blue minima to red maxima) generated with pulse parameters $\tau = 10$ fs and $F = 3$ J/cm^2. First, a cut along the y-axis in the early ∥-structures (a) and in the final flat distribution (b) caused by negative feedback with the propagated field. Second, a cut along the x-axis in the initially flat plasma distribution (c) and in the final ⊥-structures (d) amplified by positive feedback.

back loop is thereby created, amplifying ⊥-structures [see Fig. 3(d)].

In the present simulations, the symmetry is broken when light interacts with the surface roughness of the sample. For real bulk interactions, volume defects can break the symmetry to deviate from the initial and unstable flat plasma distribution. However, they must not dominate the initial plasma growth in order to avoid the formation of a strong standing wave along the propagation axis.

To summarize, the early plasma structures grow without feedback and with a pattern correctly described by the Sipe theory for transparent medium, that is $\Lambda_\parallel \sim \lambda/n$. When the plasma approaches the critical density, transverse reflections gain in importance and drive the formation of transverse resonant light modes. Negative feedback between ∥-structures and a TE mode essentially cancels the early plasma patterns. At the same time, positive feedback between ⊥-structures and a TM mode amplifies structural growth in a direction perpendicular to the original orientation [see, again, Fig 2(a)-(d)].

A few more words may be in order with respect to the origins and characteristics of the various structural patterns observed in our simulations. Details are relegated to the Supplemental Material [see SM].

In conclusion, we have simulated the growth of laser-induced plasma in the presence of a dynamical intrapulse feedback loop, absent from the current LIPSS theory. We have demonstrated how the local and dynamic nature of the interactions between plasma and light in a transparent medium are responsible for an ultrafast femtosecond self-reconfiguration of the near-surface periodic patterns. A dynamical 3D treatment of the plasma density is then necessary in order to describe properly laser-induced surface patterns on dielectrics and the intrapulse feedback dynamics. Moreover, we have achieved self-organization of plasma structures that also agree with the characteristics of laser-induced volume nanogratings, without the implementation of volume defects. Transverse mode coupling is enough to initiate the growth of the self-organized plasma structures when transverse reflections dominate over longitudinal reflections. Finally, a simple stability analysis of the feedback local effects can explain both the orientation and the periodicity of laser-induced plasma patterns.

The authors acknowledge the financial support form the Canada Excellence Research Chair in Photonics Innovations of Y. Messaddeq. We also acknowledge computational resources from Calcul Québec and the open source software Epoch.

SUPPLEMENTAL MATERIAL

The dependence of the plasma patterns periodicities with respect to the laser fluence is investigated. To precisely measure $\Lambda_\perp$ and $\Lambda_\parallel$, we first reduce the noise in the Fourier transforms by averaging over 100 simulations, each with a reshuffled surface roughness, for several values of laser fluence. We then use the maximal values along the κ_x and κ_y axes to calculate the dominant periods $\Lambda_\parallel = \lambda/(\kappa_y|_{\max})$ or $\Lambda_\perp = \lambda/(\kappa_x|_{\max})$. The results are displayed in Fig. 4.

It is clear that the nature of the final plasma patterns qualitatively change around the fluence threshold $F_{\text{th}} \sim 2$ J/cm^2. Below threshold, where feedback is weak and static mode analysis applies, we observe two distinct patterns. For $z < 50$ nm, we find structures with $\Lambda_\perp \ll \lambda$ (I) that fit the near-field interference patterns [24], also present in the Sipe theory [25]. Deeper in the sample, for $z > 50$ nm, structures with $\Lambda_\parallel \sim \lambda/n$ (III) fit the far-field interference patterns in transparent media.

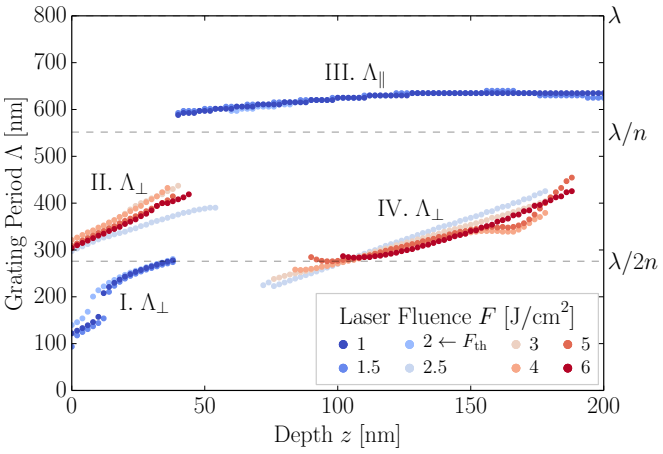

Figure 4. The grating period Λ versus depth for different values of fluence.

Above threshold, both near-field and far-field patterns shift towards a preferred periodicity of $\Lambda_\perp \sim \lambda/2n$ (II and IV). Since the plasma pattern self-reconfiguration is then dominated by transverse reflections, the natural explanation for this periodicity shift is the formation of standing waves along the x-axis [26]. Light deflected towards $+x$ and $-x$ interfere to form a standing wave with antinodes separated by half wavelengths $\lambda/2n$ at every maxima of the plasma density. The condition for positive feedback is then met at this periodicity. It is important to note that the standing wave explanation is only valid for single or few-pulse expositions. In the multiple pulse regime, interpulse feedback mechanisms come into play and have to be included explicitly, in addition to a correct intrapulse treatment, to describe the evolution of the nanogratings periodicity observed in experiments with high pulse numbers.

* Louis.Dube@phy.ulaval.ca

[1] D. Tan, K. N. Sharafudeen, Y. Yue, and J. Qiu, Progress in Materials Science **76**, 154 (2016).

[2] R. R. Gattass and E. Mazur, Nature Photonics **2**, 1749 (2008).

[3] R. Taylor, C. Hnatovsky, and E. Simova, Laser & Photonics Reviews **2**, 26 (2008).

[4] J. Qiu, K. Miura, and K. Hirao, Journal of Non-Crystalline Solids **354**, 1100 (2008).

[5] G. Vampa, T. J. Hammond, N. Thiré, B. E. Schmidt, F. Légaré, C. R. McDonald, T. Brabec, and P. B. Corkum, Nature **522**, 462 (2015).

[6] B. C. Stuart, M. D. Feit, A. M. Rubenchik, B. W. Shore, and M. D. Perry, Phys. Rev. Lett. **74**, 2248 (1995).

[7] C. Varin, C. Peltz, T. Brabec, and T. Fennel, Phys. Rev. Lett. **108**, 175007 (2012).

[8] V. R. Bhardwaj, E. Simova, P. P. Rajeev, C. Hnatovsky, R. S. Taylor, D. M. Rayner, and P. B. Corkum, Phys. Rev. Lett. **96**, 057404 (2006).

[9] J. Bonse, S. Höhm, S. V. Kirner, A. Rosenfeld, and J. Krüger, IEEE Journal of Selected Topics in Quantum Electronics **23**, 1 (2017).

[10] J. Bonse, J. Krüger, S. Höhm, and A. Rosenfeld, Journal Laser Appliations **24**, 042006 (2012).

[11] J. E. Sipe, J. F. Young, J. S. Preston, and H. M. van Driel, Physical Review B **27**, 1141 (1983).

[12] J. Bonse, A. Rosenfeld, and J. Krüger, Journal Applied Physics **106**, 104910 (2009).

[13] S. Höhm, A. Rosenfeld, J. Krüger, and J. Bonse, Journal Applied Physics **112**, 014901 (2012).

[14] R. Buschlinger, S. Nolte, and U. Peschel, Physical Review B **89**, 184306 (2014).

[15] A. Rudenko, J.-P. Colombier, and T. E. Itina, Phys. Rev. B **93**, 075427 (2016).

[16] J. Z. P. Skolski, G. R. B. E. Römer, J. Vincenc Obona, and A. J. Huis in't Veld, Journal Applied Physics **115**, 103102 (2014).

[17] J.-L. Déziel, J. Dumont, D. Gagnon, L. J. Dubé, S. H. Messaddeq, and Y. Messaddeq, Phys. Status Solidi C **13**, 121 (2016).

[18] E. G. Gamaly, A. V. Rode, B. Luther-Davies, and V. T. Tikhonchuk, Physics of Plasmas **9**, 949 (2002).

[19] F. Costache, S. Kouteva-Arguirova, and J. Reif, Applied Physics A **79**, 1429 (2004).

[20] A. Taflove and S. C. Hagness, *Computational Electrodynamics: The Finite-Difference Time-Domain Method* (Artech House, Incorporated, 2005).

[21] C. Varin, G. Bart, R. Emms, and T. Brabec, Opt. Express **23**, 2686 (2015).

[22] L. V. Keldysh, Sov. Phys. **20**, 1307 (1965).

[23] P. P. Rajeev, M. Gertsvolf, C. Hnatovsky, E. Simova, R. S. Taylor, P. B. Corkum, D. M. Rayner, and V. R. Bhardwaj, Journal of Physics B: Atomic, Molecular and Optical Physics **40**, S273 (2007).

[24] H. Zhang, J.-P. Colombier, C. Li, N. Faure, G. Cheng, and R. Stoian, Phys. Rev. B **92**, 174109 (2015).

[25] J. Z. P. Skolski, G. R. B. E. Römer, J. V. Obona, V. Ocelik, A. J. Huis in't Veld, and J. T. M. De Hosson, Physical Review B **85**, 075320 (2012).

[26] R. Buividas, L. Rosa, R. liupas, T. Kudrius, G. lekys, V. Datsyuk, and S. Juodkazis, Nanotechnology **22**, 055304 (2011).